



Published in final edited form as:

*Clin Exp Metastasis*. 2009 ; 26(5): 403–414. doi:10.1007/s10585-009-9238-y.

## Noninvasive imaging of the functional effects of anti-VEGF therapy on tumor cell extravasation and regional blood volume in an experimental brain metastasis model

Juan Juan Yin<sup>1</sup>, Kirsten Tracy<sup>1</sup>, Luhua Zhang<sup>1</sup>, Jeeva Munasinghe<sup>3</sup>, Erik Shapiro<sup>2</sup>, Alan Koretsky<sup>2</sup>, and Kathleen Kelly<sup>1</sup>

<sup>1</sup>Cell and Cancer Biology Branch, NCI

<sup>2</sup>Laboratory of Functional and Molecular Imaging, NINDS, NIH

<sup>3</sup>Mouse Imaging Facility, NINDS, NIH

### Abstract

Brain metastasis has become an increasing cause of morbidity and mortality in cancer patients as the treatment of systemic disease has improved. Brain metastases frequently are highly vascularized, a process driven primarily by VEGF. VEGF mediates numerous changes within the vasculature including endothelial cell retraction and increased permeability, vasodilation, and new vessel formation. Here we describe a xenograft brain metastasis model that mimics the critical steps of metastasis including tumor cell dissemination and vascular adhesion, tumor growth and tumor associated angiogenesis. Magnetic resonance (MR) imaging was used to evaluate two aspects of the functional response of brain metastasis to the anti-VEGF receptor therapeutic, AZD2171. MR tracking of individual cells demonstrated that AZD2171 did not impede tumor cell extravasation into the brain parenchyma despite evidence that anti-VEGF treatment decreases the permeability of the blood brain barrier. In a second assay, blood volume imaging using ultrasmall superparamagnetic iron oxide (USPIO) revealed that treatment of well-developed brain metastasis with AZD2171 for seven days led to a heterogeneous response with respect to individual tumors. Overall, there was a significant average decrease in the tumor vascular bed volume. The majority of large tumors demonstrated substantially reduced central blood volumes relative to normal brain while retaining a rim of elevated blood volume at the tumor brain interface. Small tumors or occasional large tumors displayed a static response. Models and assays such as those described here will be important for designing mechanism-based approaches to the use of anti-angiogenesis therapies for the treatment of brain metastasis.

### Keywords

animal model; blood volume; brain metastasis; MPIO; MRI; prostate cancer; USPIO

### Introduction

Brain metastases occur late in the progression of multiple types of cancers and are associated with high morbidity and mortality [1]. The exact incidence of brain metastasis is uncertain and may be clinically underestimated due to incomplete reporting and asymptomatic lesions [2]. The development of brain metastasis is estimated to occur in 10–

30% of cancer patients with solid, extracranial tumors [3]. The frequency of brain metastasis appears to be increasing, perhaps in part due to better detection. In addition, increased patient survival resulting from improved treatment of systemic disease may allow the natural history of brain metastasis to become apparent [4]. Current treatments for brain metastasis include surgery and/or radiation. These treatments usually have short-term efficacy only and associated morbidity. Targeted treatment and prevention strategies for brain metastasis are needed, and preclinical models that recapitulate the interaction of tumor cells with the unique brain microenvironment are important tools in this effort.

The genesis of brain metastases is a multistep process that includes tumor cell dissemination and migration into the brain parenchyma, establishment of micro-metastases, and tumor growth [5]. The initial steps in the metastatic cascade are potential targets for prevention therapies, while tumor growth is a target for treatment therapies. VEGF-driven angiogenesis is a common feature of brain metastasis, and there is significant interest in VEGF-targeted therapies for the treatment of primary and metastatic brain tumors [6]. VEGF functions to modify tumor vasculature via multiple mechanisms including classic sprouting angiogenesis, increased vessel permeability, vasodilation, loss of pericyte-endothelial integrity, and incorporation of bone marrow-derived endothelial progenitor cells [7].

Unique features of the brain microenvironment impact the establishment and consequences of brain metastasis. First, the blood brain barrier (BBB) is a special capillary barrier that is formed by brain microvascular endothelial cells, pericytes, and astrocytes [8]. The BBB selectively restricts the exchange of macromolecules, such as certain drugs, and some cells. Extravasation of tumor cells from the brain vasculature into the brain parenchyma is anticipated to require a specific set of properties or circumstances to interrupt the BBB. Second, the brain exhibits a high vascular density, which would be expected to influence the mechanisms whereby initiating and growing tumors obtain or maintain a vascular bed. In various preclinical models of primary or metastatic brain tumors, co-option of pre-existing vessels frequently has been observed in tumor progression or response to anti-angiogenic therapy [9]. Finally, disruption of the BBB by angiogenic mechanisms operating in tumors results in increased accumulation of peritumoral fluid. Because the brain lacks a lymphatic vasculature and is located in a confined space, this vasogenic edema results in increased intracranial pressure, a major cause of morbidity in patients with tumors in the brain [10].

Targeting blood vessels in brain tumors has been of interest given the frequent expression of VEGF in such tumors and the associated angiogenic vascular morphology and permeability changes that have been observed. However, no anti-angiogenic agent has been approved for the treatment of brain tumors. VEGF-targeted therapy has been approved for use as a single agent in renal cell carcinoma and hepatocellular carcinoma and when combined with chemotherapy for patients with metastatic colorectal, non-small-cell lung and metastatic breast cancer [7]. In a phase II study in patients with recurrent glioblastoma, the use of AZD2171, an inhibitor of the VEGF receptor and to a lesser extent the PDGF receptor tyrosine kinase activity, as a single agent led to the reversal of vascular permeability, resulting in a clinically significant reduction in vasogenic edema [10]. These studies suggest that AZD2171 is effective in modulating tumor associated vasculature in the brain and that the judicious use of anti-angiogenic agents in the brain may be achieved without fatal hemorrhagic complications. A limited number of preclinical brain metastasis studies have demonstrated that anti-VEGF treatment including anti-sense VEGF-165, PTK787, and ZD6474 caused either regression or normalization of the tumor vasculature, and in some cases, reduced the incidence of metastases [11–13].

A challenge in evaluating anti-angiogenic studies is the lack of noninvasive assay methods that correlate clinical response to therapy. Assays that provide spatial resolution of various

parameters of tumor vascularity would be particularly useful. For tumors in the brain, various dynamic MR imaging techniques following gadolinium diethylene-triaminepenta-acetic acid (Gd-DPTA) contrast agent infusion can be used to establish tumor parameters including vascular permeability, blood volume, blood flow, and mean transit time [14]. However, anti-VEGF therapy significantly decreases vascular permeability and concomitantly decreases the ability to detect tumors with Gd-DPTA [3, 15, 16]. Vascular volume is an important measure of the tumor vascular bed. Tumor vessels may be dilated or the vessel density may be different from that of the surrounding tissue, despite decreased vessel hyperpermeability following anti-VEGF treatment. Ultrasmall superparamagnetic iron oxide (USPIO) is a blood pool contrast agent that allows a sensitive determination of vascular volume [17]. USPIOs have been tested in clinical trials for detection of lymph node metastases in patients with bladder and prostate carcinoma [18, 19].

We describe here an efficient model of brain metastasis that has been developed from a human prostate cancer cell line originally isolated from a brain metastasis. This model allows the interrogation of various steps in the metastatic cascade starting with hematogenous dissemination. We couple this model with MRI techniques that visualize tumor cell dissemination and tumor vascular volume. The therapeutic effects of the anti-VEGF agent AZD2171 on these steps in the metastatic cascade were longitudinally monitored in living mice.

## Material and Methods

### Cell culture

DU145 was originally isolated from a prostate adenocarcinoma brain metastasis. The parental DU145 has low metastatic potential, and previously we have shown that DU145 cells expressing a Ras effector mutant, RasV<sup>12</sup>G<sup>37</sup>, activate the Ral-GEF pathway and promote metastasis to bone [20]. A cell line was derived from an isolated DU145/RasV<sup>12</sup>G<sup>37</sup> bone metastasis lesion by expansion in culture and subsequent FACS sorting for the marker, CD7+, which is co-expressed with Ras. The resulting cell line, DU145/RasV<sup>12</sup>G<sup>37</sup> Bone1 (DU145/RasB1) was found to be highly metastatic to both bone and brain, consistent with the phenotype of a subpopulation of cells within the DU145/RasV<sup>12</sup>G<sup>37</sup> polyclonal population. Brain metastasis occurs following cardiac inoculation of DU145/RasV<sup>12</sup>G<sup>37</sup> cells at a low but measurable rate [20]. DU145/RasB1 stably expressing GFP or RFP were produced by infecting cells with lentiGFP or lentiRFP (Biogenova, Frederick, MD), followed by FACS sorting. For bioluminescence imaging, DU145/RasB1 cells were infected with pSFGnesTGL, which encodes a GFP/luciferase/thymidine kinase fusion protein, and GFP-positive cells were isolated by FACS sorting.

### Brain metastasis model

To initiate brain metastasis,  $1 \times 10^5$  DU145/RasB1 cells in 0.1 ml PBS were inoculated into the left cardiac ventricle of male nude mice after anesthetizing with 1.5% isoflurane. Mice were weighed once per week until week 3 and twice a week thereafter and monitored for signs of morbidity. Mice were euthanized following weight loss of greater than 10% body weight or upon demonstrating brain metastasis related symptoms such as deformed calvaria, ataxic movement or other neurological abnormalities. Necropsies were performed, and mice with evidence of tumor in the chest cavity were excluded from the study as this indicated excessive leakage of tumor cells upon cardiac injection. Less than 5% of mice were excluded.

## Fresh Tissue Imaging

To image blood vessels in the brain, Dextran-conjugated Rhodamine (70,000 MW) was injected in the tail vein. After 15 min, mice were euthanized by inhalation of CO<sub>2</sub>. Brains were sectioned coronally at 1mm intervals with an acrylic matrice (Roboz, Germany), and then individual slices were examined using a Leica MZI6F stereofluorescence microscope (Leica, Germany).

## Histology

Mouse brains were collected and fixed in 10% buffered formalin and embedded in paraffin for H&E staining (HistoServ Inc., Germantown, MD). Frozen sections were used for CD31 (BD Pharmingen, San Jose, CA) and CK8 (Abcam, Cambridge, MA) staining. Frozen sections were fixed for 10 min in ice cold methanol prior to staining. Blood vessel area and blood vessel diameter were measured using a 20X lens and MetaMorph software (Molecular Devices, Downingtown, PA). Rhodamine labeled anti-rat antibody and FITC labeled anti rabbit antibody were used for fluorescence imaging.

## Bioluminescent imaging and analysis

Mice were anesthetized with 1.5% isoflurane. D-luciferin (Caliper Life Sciences, Mountain View, CA) was injected intraperitoneally at 150 mg/kg body weight 5 min before imaging. To monitor the development of brain metastasis, mice were imaged weekly using an IVIS Imaging System (Caliper Life Sciences). Analyses were performed using LivingImage software (Caliper Life Sciences) by measuring the photon flux within a region of interest drawn around the bioluminescence signals in the brain.

## MR imaging

All MRI experiments were performed on a 7-T (Bruker Avance, Billerica, MA), 21 cm horizontal scanner. The mice were anesthetized with 1.5% isoflurane and placed in a stereotaxic holder. This device was then mounted in a 72 mm volume (transmit)/25 mm surface (receive) radio frequency coil ensemble. The body core temperature was maintained at 37°C using a circulating water pad and monitored by means of a rectal temperature probe. A line through the tail vein was placed for contrasting agent infusion. Three mutually perpendicular slices were acquired through the brain as scout images.

To trace the dissemination of individual cells and subsequent tumor progression, DU145/RasB1 cells were labeled with micron-sized particles of iron oxide (MPIO). 100µl of P(S/V-COOH)Mag/Encapsulated (480,520) dragon green or (540,600) suncoast yellow 1.63 nm MPIOs (Bangs Laboratories, Inc., Fishers, IN) were incubated with cells overnight and then rinsed 3 times with PBS to remove the free MPIOs. Cells were trypsinized, gently rotated for 1 hour at room temperature, and subsequently purified using partitioning in a magnetic field for 5 minutes. Generally more than 95% of the cells were labeled after separation. To visualize MPIO particles, 3-D gradient echo images of the entire brain were acquired using a flow compensated gradient echo (GE) sequence (Echo time (TE)/repetition time (TR)=5/30 ms, number of averages (NA)=2, iso-tropic resolution=100 µm, total imaging time ~ 36 min). To count MPIO labeled cells in the brain, 3D images were viewed coronally using the Amira software (Visage Imaging, Inc., Carlsbad, CA) by scrolling through all brain slices. Hypo-intensive spots that appeared in the same position for at least two serial slices were counted. Line scans were used to measure the intensity of hypo-intensive spots. A single MRI image was uploaded using Image J software (public domain). A straight line was drawn across the brain through the hypo-intensive spot. The intensity was calculated by Image J and data transferred to GraphPad Prism (GraphPad Software, Inc., La Jolla, CA) for graphing.

To image blood volume, Ultrasmall Superparamagnetic Iron Oxide (USPIO) (Molday Iron, Biopal, Worcester, MA) was used as a contrast agent. A contiguous set of 16 T<sub>2</sub> weighted axial slices were acquired using a fast spin-echo sequence to delineate anatomical details (in-plane resolution=75 μm, TE/TR= 12.5 ms/3000 ms, echo train length=8 and NA=8). Two sets of 1 mm thick, T<sub>2</sub>\* weighted 2-D GE images, encompassing the whole brain (16 slices), were acquired (TR/TE=200/5 ms, flip angle=30°, NA=8) before and 5 min after USPIO injection. MRI data were processed and analyzed using software routines written in MATLAB (Mathworks Inc., Natic, MA). To calculate rCBV, raw data was processed with the following formula: rCBV=log (pre USPIO intensity/post USPIO intensity). Regions of interest (ROI) were drawn over each tumor. For each ROI, an identical ROI was placed in the normal contralateral section of the same brain slice. Mean rCBV values were calculated for each tumor as well as its normal contralateral region, creating an average rCBV for each tumor and for its normal brain region. To compare the blood volume change for each brain lesion over time, the ratio of the tumor rCBV over the contralateral normal rCBV at each time was used.

To image excised brains, the mice were perfused with saline and 10% formaldehyde and brains were removed and placed in 10% formaldehyde for 24 hours. The surface moisture of a brain was minimized and then submerged in Fomblin (Ausimont, NJ, USA) in a 12 mm NMR tube. The sample was then centered in a 13 mm, 3 turn solenoid coil. A fast spin echo image sequence with a TR/TE=1800/9.2 ms and 8 echos, NA=2, was used to achieve a 50 μm isotropic resolution 3-D image.

### Treatment of brain metastasis with AZD2171

The VEGFR antagonist AZD2171 was obtained from AstraZeneca Pharmaceuticals. For *in vivo* study, AZD2171 was suspended in 1% (w/v) aqueous polysorbate 80 (Sigma) and dosed at 0.1 mL/10 g of body weight per gavage. To image the effect of AZD2171 on tumor cells dissemination, six mice were inoculated with MPIO-labeled DU145/RasB1 cells. Three mice were treated with AZD2171 by daily gavage, while the other three received vehicle. To image the effect of AZD2171 on angiogenesis, mice with brain metastasis were first confirmed by bioluminescence imaging. Four weeks after tumor cell inoculation, seven mice with similar signal intensity were randomized into two groups. The mice were scanned for baseline blood volume before AZD2171 treatment. Three mice were treated with AZD2171, while the other four mice received vehicle. Five to seven days later, mice were imaged again for blood volume. Mice were then euthanized for histology.

### Data analysis

Results are expressed as mean ± SEM. Data were analyzed using Prism software (GraphPad Software, Inc. San Diego, CA) by t-test. *P* < 0.05 was considered significant.

## Results

### Systemic vascular initiation of a brain metastasis model

Following inoculation of DU145/RasB1 cells into the left cardiac ventricle, approximately 90% of animals developed brain metastasis. The average number of brain metastases per animal was 7.9±1.5 (n=12) as determined by examination of serial histological sections. Mice developed neurological symptoms around 4 weeks that included staggering gait, poor balance, and head twisting. The majority of animals also demonstrated bulging of the fontanelles, indicating elevated intracranial pressure. Animals became morbid and required euthanasia between 4 and 6 weeks. Using BL imaging, we determined that >90% of animals contained one or more bone metastases, as expected from the properties of the polyclonal population from which the DU145/RasB1 clone was derived. The morbidity associated with

bone metastasis, paraplegia, occurs two to three weeks later than brain-associated neurological symptoms and did not have any obvious impact upon the modeling of brain metastasis. Almost all animals were euthanized due to symptoms associated with brain metastasis.

As determined by histology and MR imaging, brain metastases had no preference for development in a specific brain region (Fig. 1a). The growth characteristics of the brain metastases were heterogeneous. Half of the tumors grew as solid expanding nodules, while the rest grew in an infiltrative manner closely adjacent to blood vessels (Fig. 1a, b). On high power (10X) microscopic examination, the solid metastatic nodules were not well circumscribed, as small nests of tumor cells could be seen invading adjacent brain tissue (Fig. 1b). Eighty-five percent of tumors were located in the cerebrum with the remainder in the cerebellum and olfactory regions (Fig. 1a, c). Immunohistochemical detection of tumor cell and endothelial cells with antibodies directed to CK8 and CD31 respectively, showed that the blood vessels were centered in the middle of tumor cell clusters, suggesting that tumor cells were growing around and not inside vessels (Fig. 1d).

VEGF-A is highly expressed in most primary and metastatic brain tumors. Conditioned supernatants from DU145/RasB1 cell cultures contained demonstrable levels of VEGF, PDGF-BB, and angiogenin, but no angiopoietin-2, EGF, bFGF, HB-EGF, leptin, or PIGF (data not shown). Consistent with VEGF production in DU145/RasB1 brain metastases, CD31-stained vessels were hypertrophic and dilated in both solid and infiltrative metastases (Fig. 2a). Histo-morphometric analysis showed that in comparing brain metastases to normal brain, the total blood vessel area and the vessel diameter were significantly increased in metastatic lesions (Fig. 2b). The absolute vessel density between metastases and the highly vascular normal brain was not significantly different (Fig. 2b).

### Tumor cell dissemination, intravasation, and micrometastasis formation

One therapeutic prevention strategy for brain metastasis involves targeting the initial steps, including adhesion to brain vasculature and intravasation through the blood brain barrier, of systemic tumor cell spread. It would be optimal to track such early steps of the metastatic process with non-invasive techniques. The properties of the initial steps of brain metastasis development in the model presented in this study first were established using histologic techniques. At various times after inoculation, DU145/RasB1 cells stably expressing either green fluorescent protein (GFP) or red fluorescent protein (RFP) were observed in multiple thick sections of fresh brain tissue *ex vivo*. The vasculature was visualized with fluorescently-labeled 70kD dextran. When brains were examined between 3–5 days after inoculation (Fig. 3a), individual RFP-expressing cells were observed inside brain capillaries. At 10–14 days after inoculation, individual cells were no longer obvious and small micrometastases were observed adjacent to blood capillaries in the brain parenchyma (shown in Fig. 3b as GFP-expressing DU145/RasB1). No micrometastases inside the blood vessels were found after examining 10 mice, suggesting that the tumor cells extravasated through the blood brain barrier prior to dividing. However, there is a possibility that tumor cells could have grown within the blood vessel and expanded out after breaching the vessel. To analyze the clonality of brain metastases, DU145/RasB1-GFP and DU145/RasB1-RFP cells were mixed in equal proportion prior to inoculation. Four weeks after inoculation, twenty tumors in 5 mice were observed using stereo-fluorescence microscopy, and all brain metastatic tumors were either entirely GFP or RFP expressing. No mixed tumors were found. Sixty percent of tumors were GFP-labeled and 40 % were RFP-labeled, indicating that all the tumors observed originated from single disseminated cells (Fig. 3c).

To noninvasively track the localization and intravasation of individual tumor cells, DU145/RasB1 cells were labeled with MPIOs prior to inoculation and subsequently observed using

MR imaging (Fig. 4a). MPIO labeling occurs as a result of spontaneous phagocytosis upon the incubation of particles with cells [21]. MPIO particles disrupt the magnetic field sufficiently to allow the detection of single cells [22]. For the brain MR images shown in Fig. 4a at 10 days post injection of MPIO-labeled cells, hypo-intensive spots, corresponding to MPIO-labeled cells, were obvious throughout the brain. Line scan analyses showed that hypo-intensive spots associated with MPIO-labeled cells had an average decrease in intensity of 60% and were readily distinguishable from non-specific dark spots associated with blood vessels or other irregularities (Fig. 4b). To confirm that MPIO-labeled cells localized similarly to non- MPIO-labeled cells, DU145/RasB1RFP cells were labeled with dragon green fluorescent MPIOs and then observed in sections of fresh brain tissue at 3 days post inoculation. Consistent with prior observations (Fig. 3a), individual cells containing MPIOs were lodged in the brain capillaries (Fig. 4c).

To follow the fate of populations of DU145/RasB1 cells introduced into the arterial circulation, individual mice were scanned at various times after inoculation of MPIO-labeled cells, and the numbers of hypointensive spots in the 3 dimensional space of the brain were determined (Fig. 4d). Approximately 150 hypointensive signals were observed initially within the brain at 5 hours after inoculation. The number of hypointensive spots decreased by about two-thirds between days 1 and 3. As we determined previously that the vast majority of inoculated cells remain intravascular in the first 3 to 5 days, this indicates that most trapped cells either exit or die within the blood vessels prior to extravasating into the brain. Between days three and 13, the number of hypointensive spots decreased by 50%. The number of spots appeared to decrease slightly and stabilize between 13 and 20 days at approximately 20 to 30 spots per brain. Based upon our prior observations of the localization of fluorescently-labeled DU145/RasB1 cells, it is likely that most of the spots observed after 10 days represent extravasated cells. To confirm that the dark spots are associated with live tumor cells, we compared the MRI images after brain metastasis formed, it was possible to trace tumor formation to individual hypointensive spots 80% of the time (n= 19 tumors) (Fig. 4e). Notice the size difference between the two MR images taken at same plane in 2 week and 4 week time points. The distorted MRI at week 4 is due to increased intracranial pressure associated with edema. To verify that inert MPIO particles had no effect upon the growth of cells, in vitro proliferation as well as metastasis formation were directly compared in parallel populations of MPIO-labeled and unlabeled cells (not shown). No inhibitory effect of MPIO labeling was observed.

The ability to penetrate the blood brain barrier (BBB) is a requisite property of cells that metastasize to brain. VEGF increases the permeability of the blood brain barrier [23]. Also, VEGF-mediated disruption of the endothelial barrier in liver and lung has been shown to increase the efficiency of experimental metastasis formation in these organs [24]. The contribution of VEGF-mediated disruption of the BBB to tumor cell extravasation in the brain has not been previously investigated. To determine whether tumor cell associated VEGF secretion contributes to the ability of DU145Ras/B1 cells to penetrate the BBB, the adherence and extravasation of DU145Ras/B1 cells following intracardiac inoculation in the absence and presence of AZD2171 was determined. AZD2171 was administered daily starting at the time of inoculation. As shown in Fig. 5, MPIO labeled cells were tracked and quantified from day 0 to day 27. AZD2171 treatment did not appear to significantly affect the number of hypo-intensive spots in the brain, implying that a VEGF independent mechanism for penetration of the BBB is operable in this cell.

### Parameters of tumor angiogenesis

The tortuous hyperpermeable vasculature that develops in response to VEGF is a characteristic feature of brain metastases. Vascular MRI techniques hold promise for improved detection of tumors, and the use of noninvasive imaging techniques are necessary

for evaluating changes in tumor vasculature during progression and in response to anti-angiogenic treatment. Current technology using gadolinium contrast agent is confounded by difficulty in separating the anti-permeability effects of anti-angiogenic agents from other vascular and anti-tumour effects. We used USPIO-enhanced MR imaging to generate regional cerebral volume (rCBV) measurements in brain metastases as compared to the contralateral regions of normal brain. In human brain tumors, USPIO as compared to gadolinium contrast agent remains intravascular in the early phase of tumor perfusion, leading to less vascular leak and a more reliable estimate of vascular volume [17]. USPIO-enhanced T2\* image revealed dark hypo-intensive regions, which were often also visible in the precontrast T2\* image as slightly less distinct hypo-intense regions, probably a result of high hemoglobin content and/or blood pooling in the tumors (Fig. 6a). Some tumors also displayed a circumferential hypo-intensity on T2\* images (see Fig. 7a). Interestingly, USPIO enhancement led to the detection of what appeared to be small metastatic lesions that were not visible in parallel T2 image (Fig. 6a). On average, the rCBV increased three to four fold in regions containing brain metastases (Fig. 6b).

To investigate whether AZD2171 treatment leads to functional changes in tumors as measured by the vascular volume of the tumor bed, rCBVs were determined as described above. Animals inoculated 4 weeks previously with DU145/RasB1 cells were imaged and then either treated daily with AZD2171 or with vehicle control. Five to seven days later, four control and three treated animals were imaged again. Representative images are shown in Figures 7a. The two metastases (marked with arrowheads) that are evident in the control animal with both T2-weighted (left panels) and USPIO contrast images (right panels) increased in size between four and five weeks. The more centrally-located tumor displayed a less intense center at the five week time point, suggesting the development of central necrosis.

Three tumors, two large and one small, are visible in the USPIO contrast images (right panels) of the AZD2171 treated animal shown in Fig. 7a. The two large tumors, marked by arrowheads, demonstrated significant decreases in vascular volume after AZD2171 treatment but retained a rim of enhanced vascular volume relative to normal brain. There appeared to be an additional small tumor (marked by an arrow) that remained static with treatment. It was not possible to discern a response of the large tumors to AZD2171 treatment in the T2-weighted morphology scans (left panels), demonstrating the importance of functional imaging. Noticeably, the brain MR image at post-treatment is bulging and distorted compared with that of the pre-treatment. This is an indication of increased intracranial pressure associated with edema. However, the pre – and post- treatment MR images in AZD2171 treated mouse are relatively same. The rCBV images of large tumors are consistent with a common histological phenotype that can be discerned following AZD2171 treatment as shown in 7b, namely regression of central CD31 stained vessels and retention of CD31 hypertrophic blood vessels at the tumor-brain interface. Another post-treatment rCBV phenotype is shown in 7c whereby slightly decreased blood volume in the center of the tumor is accompanied by an increased peripheral area of higher blood volume, consistent with peripheral tumor expansion or invasion during treatment. Overall, AZD2171 treatment resulted in a statistically significant average decrease in the blood volume of 12 metastases evaluated in three mice (Fig. 7d). In addition, the ability to visualize the heterogeneity of responses among the metastases is anticipated to be of importance in evaluating the design of single agent and combination therapies.

AZD2171 decreased the morbidity of the metastasis-bearing mice treated between four and five weeks in a cohort of animals, some of which were used for the studies described above. At the end of the treatment, five of six AZD2171-treated mice demonstrated stable or increased weight and no typical signs of morbidity such as bulging fontanelles or

neurological symptoms. By comparison, two of eight control mice died before the final scan, and it was necessary to euthanize the remaining six untreated mice directly after the final scan.

## Discussion

Brain metastasis is recognized as an increasing clinical problem. The lack of effective treatments for brain metastasis and the limitations in obtaining patient biopsies underscore the need for preclinical models. Brain metastasis occurs most frequently in lung, melanoma, and breast cancers [4]. In addition, a recent series of autopsies found that 20% of patients with advanced prostate cancer demonstrated brain metastasis [25]. We describe here an efficient, hematogenously-disseminated model of brain metastasis derived from a human androgen-independent prostate cancer. This new model is coupled with the use of non-invasive MR imaging techniques to interrogate functional steps in response to anti-angiogenesis treatment. Brain metastases in the DU145/RasB1 model occur as large, expansive rounded lesions with marked peritumoral edema as well as small infiltrative lesions. It is not clear whether the heterogeneity arises from genetic instability, from microenvironmental influences, or from a combination of both. Given the clonal origin of the DU145/RasB1 cell line, genetic heterogeneity would have to result from an ongoing genetic or epigenetic instability. Although brain metastases generally do show tissue specific properties relating to the primary tumor source, therapeutics that target the brain microenvironment most likely will act upon multiple types of brain metastasis.

Primary and metastatic brain tumors are densely vascularized and commonly express high levels of VEGF [3]. Thus, there has been considerable interest in anti-angiogenic therapy to treat brain tumors. Anti-angiogenic therapy predominantly targets non-cancer cells, endothelial and possibly hematopoietic-derived cells, in the brain microenvironment. The lessons learned from clinical anti-VEGF therapy for advanced non-cranial tumors and from the early clinical trials of adult glioblastoma suggest that the use of anti-VEGF therapy as a single agent will result in transient responsiveness [7]. An increased understanding of the angiogenic process in the brain microenvironment is needed to pioneer new approaches. Important questions include the diversity of angiogenic inducers and mediators, the temporal sequence of potential functional responses, and the heterogeneity of responses within clonally related tumors.

A critical step for disseminated cells to initiate brain metastasis is the ability to cross the BBB into the parenchyma of the brain. The application of single cell MR imaging provides an assay to quantitatively and noninvasively determine the effect of therapeutics upon vascular arrest and extravasation through the BBB. To the best of our knowledge, the results described here are the first use of single cell MR imaging to track extravasation across the blood brain barrier *in vivo*. We have used parallel histological analyses of fluorescently-labeled cells and MR images of MPIO-labeled cells to characterize the temporal sequence of cell loss within and migration from the brain vasculature. Using MPIO-labeled DU145/RasB1 cells, we have shown that approximately, 0.1–0.3% of injected cells arrest in the vasculature of the brain. Within three to five days after inoculation, the vast majority of cells are lost from vessels in the brain as demonstrated by BL imaging, fluorescence imaging, and counting MPIO-generated voids. About 10% of the initially arrested cells, i.e. 0.01–0.03% of the total inoculated cells, are detectable as signal voids at a time when the majority of cells have extravasated into the brain parenchyma.

The precise mechanisms used by tumor cells to penetrate the blood brain barrier are unknown. VEGF increases the permeability of the BBB to small molecules and has been shown to disrupt the VE-cadherin- $\beta$ -catenin junctional complexes [26]. One possibility that

has been suggested is that VEGF produced by tumor cells arrested in the brain microvasculature induces endothelial cell retraction and exposure of the vascular basement membrane [27]. Subsequently, proteolytic activity expressed by the tumor cells enables extravasation. Although the role of VEGF in tumor cell extravasation has not been extensively investigated, two studies support this hypothesis. First, the ability of MDA-MB-231 cells to penetrate a human BMEC monolayer in vitro was inhibited by pretreatment with the VEGF receptor inhibitor, SU-1498 [28]. Second, a single treatment of VEGF inhibitor or VEGFR-2 inhibitor at the time of venous inoculation of CT26 colon carcinoma cells stabilized endothelial cell barrier function and inhibited experimental micrometastasis formation in the lung [24]. By contrast, we did not see a demonstrable effect of AZD2171 on DU145/RasB1 extravasation from the brain vasculature. Other molecules such as 12 (S) hydroxyicosatetraenoic acid (HETE) have been shown to induce endothelial retraction [27]. Perhaps DU145/RasB1 cells produce molecules with redundant endothelial retracting activity to that of VEGF. Although the experiments shown here do not support a necessary role for VEGF in extravasation of DU145/RASB1 tumor cells through the BBB, we anticipate that the ability to image single metastatic cells in the brain will have wide utility in experimental models.

It should be pointed out that there is uncertainty as to whether the MPIO labeling technique will be useful for tumor cell dormancy studies [29]. Of the approximately 30 signal voids representing MPIO-labeled DU145/RasB1 cells that can be detected at day ten, 15–20% develop into metastatic brain tumors. Due to the technological challenge of histologically-locating single MPIO-containing cells within the volume of the whole brain, it is unclear whether the approximately 25 remaining MPIO-generated signal voids represent dormant cells, arrested micrometastases, remnant particles from nonviable cells, or a combination of the above.

The transient growth inhibitory response of tumors to anti-VEGF therapy has focused current and future investigations toward a mechanistic understanding of modes of tumor resistance. Non-invasive assays to measure functional properties of tumor vasculature are needed. As shown here, USPIO enhanced MR imaging provides a quantitative and spatially-resolved measure of the tumor vasculature blood volume. Non-treated tumors clearly demonstrated within a one week period increased tumor volume that could be resolved as an expanded area of increased rCBV. By contrast, AZD2171 treatment resulted in a decreased blood volume within the center of the large tumors below that of the contralateral normal brain vascular volume. However, the angiogenic response at the tumor-brain interface was not affected by AZD2171. Histological sections confirmed central necrosis of large tumors and that the blood vessels at the rim of the AZD2171 treated tumor were still dilated, and endothelial cells remained hypertrophic. How tumor vessels on the periphery differ from those in the interior is of interest. One possibility is that factors supplied by the normal brain microenvironment or invading hematopoietic cells make peripheral vessels less susceptible to anti-VEGF effects. Another possibility is that peripheral vessels have still retained some morphological properties of normal vessels such as pericyte coverage that render them less sensitive to VEGFR, or possibly PDGFR, inhibition [30]. There was additional heterogeneity in the response of tumors to anti-VEGF treatment, similar to what might be expected in patient responses to therapy. After one week of AZD2171 treatment, some small tumors appeared relatively unchanged, and some large tumors increased their invasion into normal brain. Such heterogeneity combined with longitudinal imaging is anticipated to be very informative in mechanistic analyses of responses to sequentially applied therapies.

## References

1. Fidler IJ, Yano S, Zhang RD, et al. The seed and soil hypothesis: vascularisation and brain metastases. *Lancet Oncol.* 2002; 3 (1):53–7. [PubMed: 11905606]
2. Posner JB. Management of brain metastases. *Rev Neurol (Paris).* 1992; 148 (6–7):477–87. [PubMed: 1448668]
3. Jain RK, di Tomaso E, Duda DG, et al. Angiogenesis in brain tumours. *Nat Rev Neurosci.* 2007; 8 (8):610–22. [PubMed: 17643088]
4. Palmieri D, Chambers AF, Felding-Habermann B, et al. The biology of metastasis to a sanctuary site. *Clin Cancer Res.* 2007; 13 (6):1656–62. [PubMed: 17363518]
5. Chambers AF, Groom AC, MacDonald IC. Dissemination and growth of cancer cells in metastatic sites. *Nat Rev Cancer.* 2002; 2 (8):563–72. [PubMed: 12154349]
6. Lakka SS, Rao JS. Antiangiogenic therapy in brain tumors. *Expert Rev Neurother.* 2008; 8 (10):1457–73. [PubMed: 18928341]
7. Ellis LM, Hicklin DJ. VEGF-targeted therapy: mechanisms of anti-tumour activity. *Nat Rev Cancer.* 2008; 8 (8):579–91. [PubMed: 18596824]
8. Johansson BB. The physiology of the blood-brain barrier. *Adv Exp Med Biol.* 1990; 274:25–39. [PubMed: 2239426]
9. Bergers G, Hanahan D. Modes of resistance to anti-angiogenic therapy. *Nat Rev Cancer.* 2008; 8 (8):592–603. [PubMed: 18650835]
10. Batchelor TT, Sorensen AG, di Tomaso E, et al. AZD2171, a pan-VEGF receptor tyrosine kinase inhibitor, normalizes tumor vasculature and alleviates edema in glioblastoma patients. *Cancer Cell.* 2007; 11 (1):83–95. [PubMed: 17222792]
11. Kim LS, Huang S, Lu W, et al. Vascular endothelial growth factor expression promotes the growth of breast cancer brain metastases in nude mice. *Clin Exp Metastasis.* 2004; 21 (2):107–18. [PubMed: 15168728]
12. Leenders WP, Kusters B, Verrijp K, et al. Antiangiogenic therapy of cerebral melanoma metastases results in sustained tumor progression via vessel co-option. *Clin Cancer Res.* 2004; 10 (18 Pt 1):6222–30. [PubMed: 15448011]
13. Yano S, Shinohara H, Herbst RS, et al. Expression of vascular endothelial growth factor is necessary but not sufficient for production and growth of brain metastasis. *Cancer Res.* 2000; 60 (17):4959–67. [PubMed: 10987313]
14. Price SJ. The role of advanced MR imaging in understanding brain tumour pathology. *Br J Neurosurg.* 2007; 21 (6):562–75. [PubMed: 18071983]
15. Claes A, Gambarota G, Hamans B, et al. Magnetic resonance imaging-based detection of glial brain tumors in mice after antiangiogenic treatment. *Int J Cancer.* 2008; 122 (9):1981–6. [PubMed: 18081012]
16. Jain RK. Normalization of tumor vasculature: an emerging concept in antiangiogenic therapy. *Science.* 2005; 307 (5706):58–62. [PubMed: 15637262]
17. Neuwelt EA, Varallyay CG, Manninger S, et al. The potential of ferumoxytol nanoparticle magnetic resonance imaging, perfusion, and angiography in central nervous system malignancy: a pilot study. *Neurosurgery.* 2007; 60(4):601–11. discussion 11–2. [PubMed: 17415196]
18. Corot C, Robert P, Idee JM, et al. Recent advances in iron oxide nanocrystal technology for medical imaging. *Adv Drug Deliv Rev.* 2006; 58 (14):1471–504. [PubMed: 17116343]
19. Harisinghani MG, Barentsz J, Hahn PF, et al. Noninvasive detection of clinically occult lymph-node metastases in prostate cancer. *N Engl J Med.* 2003; 348 (25):2491–9. [PubMed: 12815134]
20. Yin J, Pollock C, Tracy K, et al. Activation of the RalGEF/Ral pathway promotes prostate cancer metastasis to bone. *Mol Cell Biol.* 2007; 27 (21):7538–50. [PubMed: 17709381]
21. Shapiro EM, Skrtic S, Koretsky AP. Sizing it up: cellular MRI using micron-sized iron oxide particles. *Magn Reson Med.* 2005; 53 (2):329–38. [PubMed: 15678543]
22. Shapiro EM, Skrtic S, Sharer K, et al. MRI detection of single particles for cellular imaging. *Proc Natl Acad Sci U S A.* 2004; 101 (30):10901–6. [PubMed: 15256592]

23. Dobrogowska DH, Lossinsky AS, Tarnawski M, et al. Increased blood-brain barrier permeability and endothelial abnormalities induced by vascular endothelial growth factor. *J Neurocytol.* 1998; 27 (3):163–73. [PubMed: 10640176]
24. Weis S, Cui J, Barnes L, et al. Endothelial barrier disruption by VEGF-mediated Src activity potentiates tumor cell extravasation and metastasis. *J Cell Biol.* 2004; 167 (2):223–9. [PubMed: 15504909]
25. Shah RB, Mehra R, Chinnaiyan AM, et al. Androgen-independent prostate cancer is a heterogeneous group of diseases: lessons from a rapid autopsy program. *Cancer Res.* 2004; 64 (24):9209–16. [PubMed: 15604294]
26. Weis S, Shintani S, Weber A, et al. Src blockade stabilizes a Flk/cadherin complex, reducing edema and tissue injury following myocardial infarction. *J Clin Invest.* 2004; 113 (6):885–94. [PubMed: 15067321]
27. Miles FL, Pruitt FL, van Golen KL, et al. Stepping out of the flow: capillary extravasation in cancer metastasis. *Clin Exp Metastasis.* 2008; 25 (4):305–24. [PubMed: 17906932]
28. Lee TH, Avraham HK, Jiang S, et al. Vascular endothelial growth factor modulates the transendothelial migration of MDA-MB-231 breast cancer cells through regulation of brain microvascular endothelial cell permeability. *J Biol Chem.* 2003; 278 (7):5277–84. [PubMed: 12446667]
29. Heyn C, Ronald JA, Ramadan SS, et al. In vivo MRI of cancer cell fate at the single-cell level in a mouse model of breast cancer metastasis to the brain. *Magn Reson Med.* 2006; 56 (5):1001–10. [PubMed: 17029229]
30. Wedge SR, Kendrew J, Hennequin LF, et al. AZD2171: a highly potent, orally bioavailable, vascular endothelial growth factor receptor-2 tyrosine kinase inhibitor for the treatment of cancer. *Cancer Res.* 2005; 65 (10):4389–400. [PubMed: 15899831]

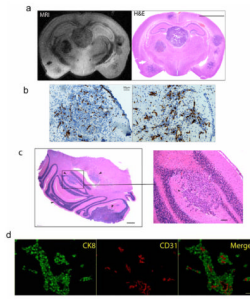


**Figure 1. Histological characterization of the DU145/RasB1 brain metastasis model**

a. A high resolution coronal MRI section obtained on a fixed brain (left panel) and matching histological section (right panel) from an animal with multiple brain metastasis; (scale bar =2.5 mm). b. Microscopic images of tumors grow as an expanding nodular (left) and invasive (right) brain metastatic lesions; (scale bar =50  $\mu$ m). Blood vessels were stained with CD31. c. Microscopic section of cerebellum with multiple metastases indicated by black arrows; (scale bar =200  $\mu$ m; cropped section: scale bar =100  $\mu$ m). d. Immunofluorescence staining of CK8 (green) and CD31 (red) on brain sections; (scale bar =50  $\mu$ m).

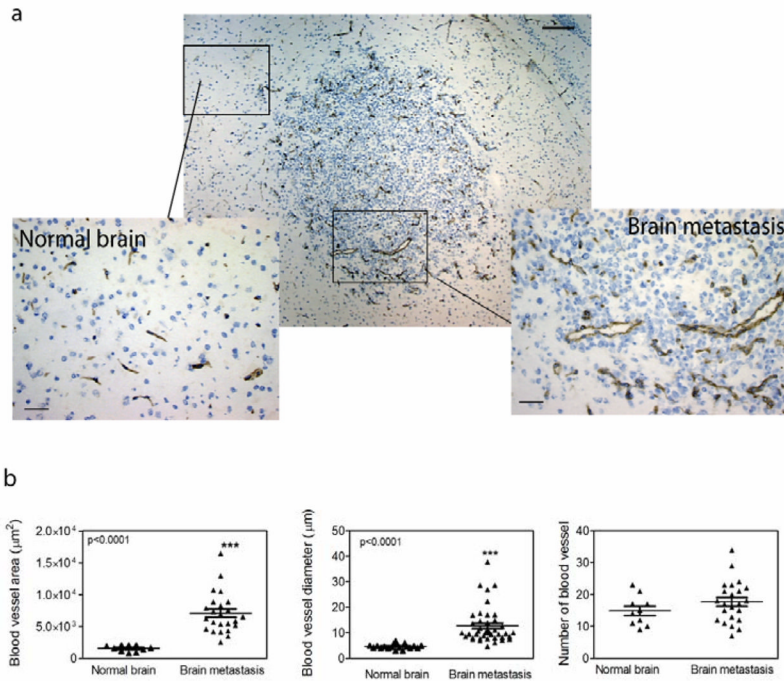


**Figure 2. Angiogenic properties of brain metastasis**

a. CD31 stained vessels within and around a metastasis in brain parenchyma; (scale bar 100  $\mu\text{m}$ ) and two cropped regions showing CD31 stained (brown) blood vessels in normal brain and a brain metastasis; (scale bar = 50  $\mu\text{m}$ ). b. Histomorphometric analysis of CD31 positive blood vessels in normal brain and metastatic lesions. Total blood vessel area, blood vessel diameter and the number of blood vessels were analyzed on 20X images.

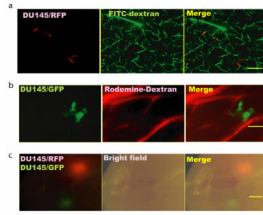


**Figure 3. Brain metastasis progression visualized by fluorescence imaging**

a. *Ex vivo* confocal image of thick brain slices showing RFP expressing DU145/RasB1 cells (red) in FITC-conjugated dextran-labeled blood vessels (green) 3 days after tumor cell inoculation; (scale bar = 100  $\mu$ m). b. Micrometastatic cluster of GFP expressing DU145/RasB1 cells (green) in the brain adjacent to rhodamine-conjugated dextran-labeled blood vessels (red) 10 days after tumor cell inoculation; (scale bar = 50  $\mu$ m). c. Two brain metastases generated from an equal mixture of GFP and RFP expressing DU145/RasB1 cells; (scale bar = 1 mm).

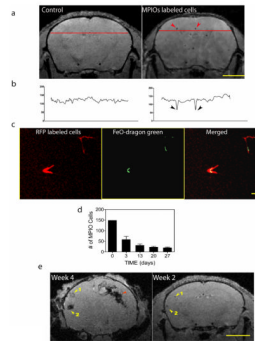


**Figure 4. Detecting single MPIO-labeled tumor cells in the brains of live mice**

a. MR image showing hypointensive spots in the brain of a mouse inoculated with MPIO-labeled cells (right). No such spots are obvious in the control mouse injected with non-MPIO-labeled cells (left); (scale bar = 2 mm). b. Line scan showing the relative intensity of background and hypointensive spots in a mouse brain containing MPIO-labeled DU145/RasB1 cells (right) compared with the brain of a control mouse. c. Fluorescent image of RFP-labeled tumor cells containing dragon green fluorescent MPIOs trapped in the brain vasculature 3 days after tumor cell inoculation; (scale bar = 25  $\mu$ m). d. Average number of hypointensive spots/brain measured in three mice, determined using 3D MRI scans at the indicated times. e. Representative example of similarly positioned MRI sections in a single mouse at 2 and 4 weeks following inoculation of MPIO-labeled cells. Yellow arrows indicate positioning of hypointensive spots and subsequently developing tumors. The red arrow indicates a brain hemorrhage caused by a brain metastasis located in an adjacent brain region; (scale bar =2 mm).

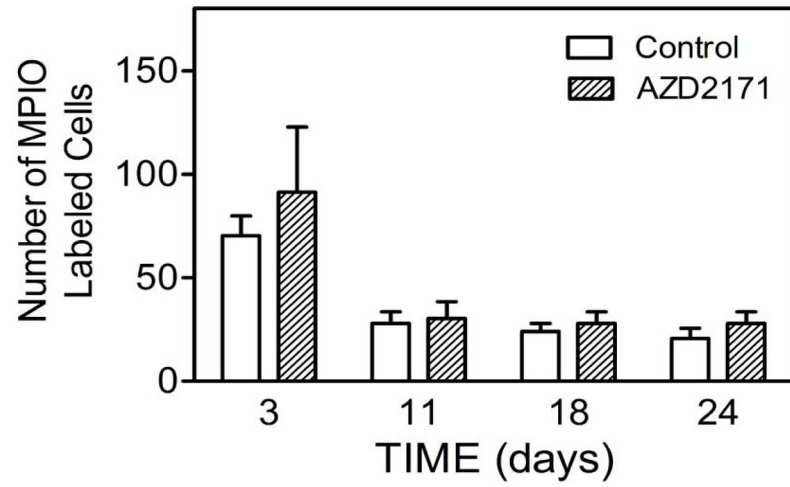


**Figure 5. The effect of AZD2171 treatment on the change of hypo-intensive spots**  
Quantification of the number of hypointensive spots/brain for control and AZD2171 treated mice from day 3 to day 24. n=3 animals per group.

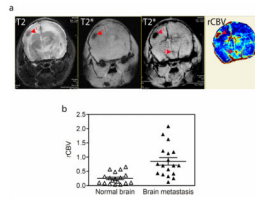


**Figure 6. Monitoring regional cerebral blood volume**

a. A T2 image of a brain with metastatic lesions (far left panel), the T2\* gradient echo MR image collected before and after USPIO injection of the same brain (middle two panels) and the matching regional cerebral blood volume (rCBV) map (far right panel); (scale bar = 2 mm). b. Relative intensity of rCBV measured in regions of brain metastasis compared with the contra-lateral region in the same brain.

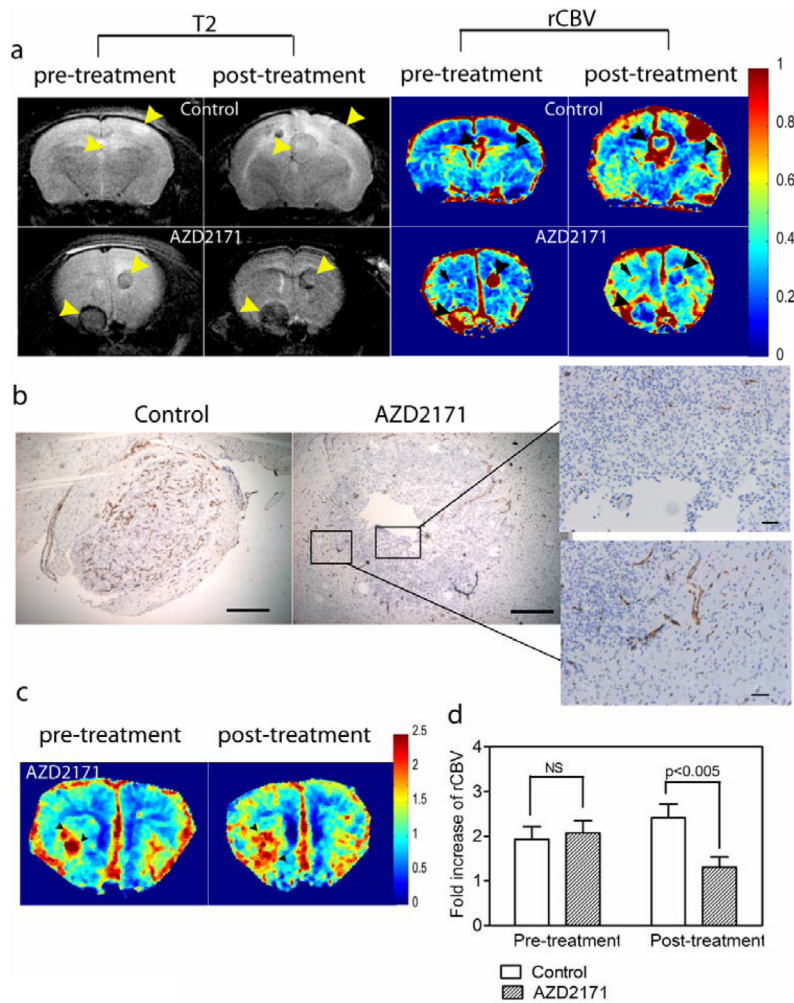


**Figure 7. Monitoring the effects of AZD2171 on brain metastasis tumor bed volume**  
 a. T2 weighted images (left 4 panels) and rCBV maps (right four panels) of representative mice from the control, vehicle-treated group (four upper panels) and the AZD2171 treatment group (four lower panels). These images show metastatic lesions from morphology scans (yellow arrowheads) and corresponding blood volume pre- and post treatment. b. CD31 staining in a representative brain metastasis from an untreated or a mouse treated with AZD2171 for seven days; (scale bar=500  $\mu$ m for un-cropped sections, scale bar=50  $\mu$ m for the cropped sections). c. rCBV map of two small brain metastases in a mouse before and after seven days of AZD2171 treatment (black arrowheads). d. The fold change of the rCBV in brain metastases relative to the contra-lateral normal brain area in untreated and AZD2171-treated mice.